Geophysical Research Letters

RESEARCH LETTER
10.1029/2019GL082887

Key Points:
- A new method is presented for calculating the terrestrial and ocean carbon feedback from observational constraints and model simulations
- The terrestrial carbon feedback is analyzed from observational reconstructions as 0.31 ± 0.09 W·m^{-2}·K^{-1}
- The total feedback from physical climate system and carbon cycle processes is 1.48 (95% range from 0.76 to 2.32) W·m^{-2}·K^{-1}

Supporting Information:
- Supporting Information S1

Correspondence to:
P. Goodwin,
p.a.goodwin@soton.ac.uk

Citation:
Goodwin, P., Williams, R. G., Roussenov, V. M., & Katavouta, A. (2019). Climate sensitivity from both physical and carbon cycle feedbacks. *Geophysical Research Letters*, *46*, 7554–7564. https://doi.org/10.1029/2019GL082887

Received 18 MAR 2019
Accepted 12 JUN 2019
Accepted article online 22 JUN 2019
Published online 1 JUL 2019

Climate Sensitivity From Both Physical and Carbon Cycle Feedbacks

Philip Goodwin[1], Richard G. Williams[2], Vassil M. Roussenov[2], and Anna Katavouta[2]

[1]Ocean and Earth Science, National Oceanography Centre Southampton, University of Southampton, Southampton, UK,
[2]Department of Earth, Ocean and Ecological Sciences, School of Environmental Sciences, University of Liverpool, Liverpool, UK

Abstract The surface warming response to anthropogenic forcing is highly sensitive to the strength of feedbacks in both the physical climate and carbon cycle systems. However, the definitions of climate feedback, $\lambda_{\mathrm{Climate}}$ in W·m^{-2}·K^{-1}, and climate sensitivity, S_{Climate} in K/(W/m^2), explicitly exclude the impact of carbon cycle feedbacks. Here we provide a new framework to incorporate carbon feedback into the definitions of climate feedback and sensitivity. Applying our framework to the Global Carbon Budget reconstructions reveals a present-day terrestrial carbon feedback of $\lambda_{\mathrm{Carbon}} = 0.31 \pm 0.09$ W·m^{-2}·K^{-1} and an ocean carbon feedback of −0.06 to 0.015 W·m^{-2}·K^{-1} in Earth system models. Observational constraints reveal a combined climate and carbon feedback of $\lambda_{\mathrm{Climate+Carbon}} = 1.48$ W·m^{-2}·K^{-1} with a 95% range of 0.76 to 2.32 W·m^{-2}·K^{-1} on centennial time scales, corresponding to a combined climate and carbon sensitivity of $S_{\mathrm{Climate+Carbon}} = 0.67$ K/(W/m^2) with a 95% range of 0.43 to 1.32 K/(W/m^2).

Plain Language Summary Feedback processes in the physical climate system and the carbon cycle affect the Earth's climate response to emissions of greenhouse gases, such as carbon dioxide. Physical climate feedbacks include the responses of clouds and atmospheric water vapor to rising surface temperatures, while carbon cycle feedbacks affect how much of the emitted carbon dioxide is removed from the atmosphere and stored in the ocean and on land. Conventionally, definitions of climate feedback and climate sensitivity include all the feedbacks in the physical climate system but do not include carbon cycle feedbacks. This study provides a new framework to incorporate carbon feedback into the definitions of climate feedback and sensitivity. Evaluating the historical strengths of physical climate system and carbon cycle feedbacks suggests emissions of carbon dioxide will cause equilibrium (century time scale) surface warming to increase between 0.6 and 2.0 °C for every 1,000 PgC emitted when an equilibrium is approached between the atmosphere and the ocean over many centuries.

1. Introduction

Climate change is driven by a combination of radiative forcing and climate feedbacks operating in the climate system (see review in Knutti et al., 2017). The climate feedback is usually expressed in terms of the change in surface temperature multiplied by a feedback parameter, λ in W·m^{-2}·K^{-1}, defined in terms of a wide range of physical processes, including the Planck response of enhanced longwave emission from a warmer surface and physical feedbacks from changes in water vapor, lapse rate, cloud cover, and ice albedo (Andrews et al., 2012; Andrews et al., 2015; Armour et al., 2013; Ceppi & Gregory, 2017; Gregory et al., 2004). In contrast, the carbon cycle responses and feedbacks are usually defined in terms of how atmospheric carbon dioxide and temperature linearly combine to alter the carbon inventories of the climate system (Arora et al., 2013; Friedlingstein et al., 2003, 2006), which may be expressed in terms of a radiative feedback parameter in W·m^{-2}·K^{-1} (Gregory et al., 2009). However, there are difficulties in applying this carbon feedback method due to nonlinearities in how the separate atmospheric carbon dioxide and temperature effects combine together (Schwinger et al., 2014) giving rise to errors in the overall carbon feedback (Arora et al., 2013). This linearization method also cannot be used to calculate the carbon feedback directly from observational reconstructions of the carbon cycle (e.g., le Quéré et al., 2018), since there is no observational method to generate the hypothetical state with a range of feedback processes turned off for the real world.

The separation of forcing and feedback is dependent upon the nature of the climate perturbation. In climate model experiments driven by an imposed atmospheric CO_2 trajectory, a radiative forcing is provided from the increase in atmospheric CO_2 that automatically includes the effects of carbon cycle feedbacks. In

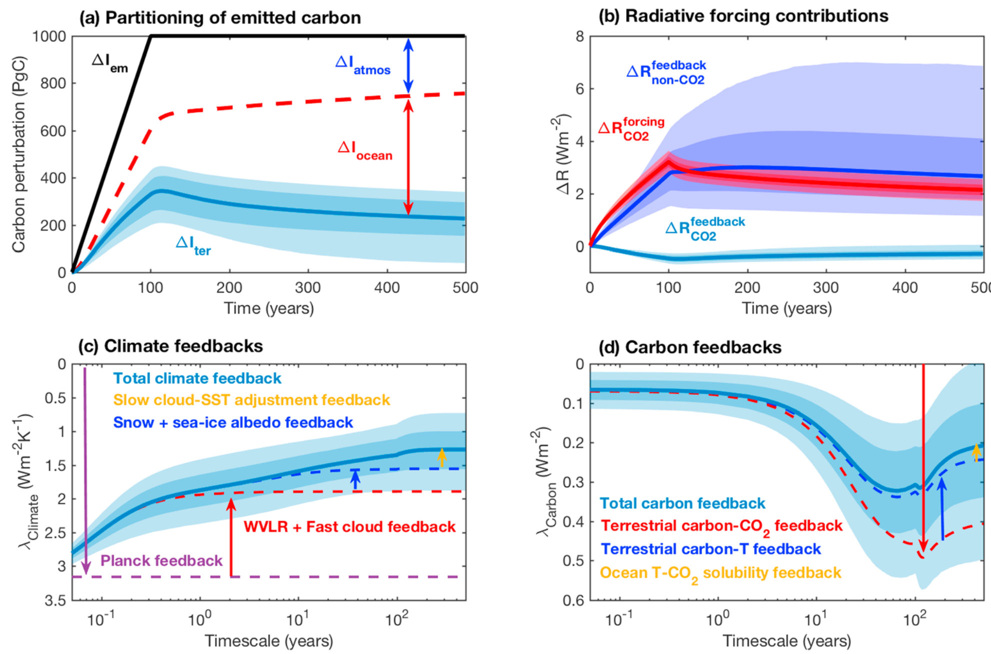

Figure 1. Climate and carbon feedback over time for a 1,000 PgC emission experiment in a large ensemble of observation-constrained simulations. (a) Partitioning of a 1,000 PgC carbon emission (ΔI_{em}, black line) between the terrestrial carbon (ΔI_{ter}, light blue line and shading), ocean (ΔI_{ocean}, red arrow), and atmospheric inventories (ΔI_{atmos}, bright blue arrow). (b) Radiative forcing contributions from the CO_2 forcing from emissions without carbon feedbacks (red), plus the non-CO_2 feedbacks (blue), and from the carbon feedbacks (light blue). (c) Total climate feedback, $\lambda_{Climate}$ (light blue line and shading), and (d) total carbon feedback, λ_{Carbon} (light blue line and shading), both showing contributions from individual feedback processes (dashed lines and arrows). On all panels, lines show the ensemble median, dark shading is 66% range, and light shading is the 95% range.

contrast, for climate model experiments driven by carbon emissions, a radiative forcing is provided from the increase in atmospheric CO_2 directly caused by the carbon emission together with a radiative feedback from the change in atmospheric CO_2 caused by changes in the terrestrial and ocean carbon reservoirs.

To understand this distinction between forcing and feedback, consider the response of a conceptual Earth system model to a pulse of carbon released to the atmosphere, which is partitioned between the atmosphere, ocean, and terrestrial systems (Figure 1a). The original carbon release drives a radiative forcing from the increase in atmospheric CO_2 (Figure 1b, red line), which is augmented by a radiative feedback from both non-CO_2 and CO_2 changes (Figure 1b). These feedbacks may act to enhance or oppose the original forcing perturbation.

Our aim is to define and evaluate a new feedback parameter for the carbon system that

1. takes into account the combined effects of the non-CO_2 and CO_2 feedbacks operating in the climate system, thus avoiding the need to make a linearizing assumption that introduces error;
2. allows direct comparison between magnitudes of, and uncertainties in, feedbacks in the climate and carbon systems; and
3. allows the practical application of real-world observational data to analyze carbon feedback.

2. Definition of a Climate and Carbon Feedback Parameter

Consider the global energy balance for a climate system perturbed from an initial steady state (e.g., Figures 1a and 1b). The radiative forcing perturbation, $\Delta R'$, from the original forcing perturbation combined with subsequent feedback terms is balanced by additional outgoing longwave radiation emitted due to surface warming, $\lambda_{Planck}\Delta T$, and the net Earth system heat uptake, N, all terms defined in W/m^2,

$$\Delta R' = \lambda_{\mathrm{Planck}} \Delta T + N, \tag{1}$$

where $\lambda_{\mathrm{Planck}}$ is the Planck feedback parameter in $\mathrm{W{\cdot}m^{-2}{\cdot}K^{-1}}$ and ΔT is the change in global-mean surface temperature in K. The radiative forcing, $\Delta R'$, consists of an original forcing perturbation, $\Delta R^{\mathrm{forcing}}$ plus a subsequent feedback term, $\Delta R^{\mathrm{feedback}}$, $\Delta R' = \Delta R^{\mathrm{forcing}} + \Delta R^{\mathrm{feedback}}$, and the feedback may be written in terms of the separate non-CO_2 and CO_2 components, $\Delta R^{\mathrm{feedback}}_{\mathrm{non-CO2}}$ and $\Delta R^{\mathrm{feedback}}_{\mathrm{CO2}}$, respectively (Figure 1b), such that

$$\Delta R' = \Delta R^{\mathrm{forcing}} + \Delta R^{\mathrm{feedback}}_{\mathrm{non-CO2}} + \Delta R^{\mathrm{feedback}}_{\mathrm{CO2}}. \tag{2}$$

The radiative feedback term from non-CO_2 feedbacks, $\Delta R^{\mathrm{feedback}}_{\mathrm{non-CO2}}$, includes the effects of changes in water vapor, lapse rate, clouds, and surface albedo, while the radiative feedback term from CO_2, $\Delta R^{\mathrm{feedback}}_{\mathrm{CO2}}$, includes how radiative forcing from atmospheric CO_2 is altered by changes in the ocean and terrestrial carbon inventories.

The radiative response is often defined in terms of a climate feedback, $\lambda_{\mathrm{Climate}}\Delta T$ in $\mathrm{W/m^2}$, by combining the Planck response, $\lambda_{\mathrm{Planck}}\Delta T$, with the radiative forcing from non-CO_2 feedbacks, $\Delta R^{\mathrm{feedback}}_{\mathrm{non-CO2}}$ (e.g., see Intergovernmental Panel on Climate Change, 2013; Knutti et al., 2017),

$$\lambda_{\mathrm{Climate}} \Delta T = \lambda_{\mathrm{Planck}} \Delta T - \Delta R^{\mathrm{feedback}}_{\mathrm{non-CO2}}, \tag{3}$$

such that the energy balance in (1) may be reexpressed from (2) and (3) by

$$\Delta R^{\mathrm{forcing}} + \Delta R^{\mathrm{feedback}}_{\mathrm{CO2}} = \lambda_{\mathrm{Planck}} \Delta T - \Delta R^{\mathrm{feedback}}_{\mathrm{non-CO2}} + N = \lambda_{\mathrm{Climate}} \Delta T + N. \tag{4}$$

The standard form of the climate feedback definition in (3) does not encapsulate the full sensitivity of the Earth system to perturbation, as the definition only accounts for the strength of the non-CO_2 feedbacks in the system and ignores the impact of carbon cycle feedbacks, which are instead treated as part of the forcing perturbation in (4). Here, we reexpress the energy balance relations (1) and (4) using a new combined carbon plus climate feedback, $\lambda_{\mathrm{Climate+Carbon}}$ in $\mathrm{W{\cdot}m^{-2}{\cdot}K^{-1}}$, defined as the sum of the climate and carbon feedbacks,

$$\lambda_{\mathrm{Climate+Carbon}} \Delta T = \lambda_{\mathrm{Planck}} \Delta T - \Delta R^{\mathrm{feedback}}_{\mathrm{non-CO2}} - \Delta R^{\mathrm{feedback}}_{\mathrm{CO2}} = (\lambda_{\mathrm{Climate}} + \lambda_{\mathrm{Carbon}}) \Delta T, \tag{5}$$

where $\lambda_{\mathrm{Carbon}} = -\Delta R^{\mathrm{feedback}}_{\mathrm{CO2}} / \Delta T$. The energy balance in (1) may now be more explicitly written in terms of the original radiative forcing, $\Delta R^{\mathrm{forcing}}$, balancing the radiative response from the combined climate and carbon responses, $\lambda_{\mathrm{Climate+Carbon}}\Delta T$, plus the planetary heat uptake, N, such that

$$\Delta R^{\mathrm{forcing}} = \lambda_{\mathrm{Climate}} \Delta T - \Delta R^{\mathrm{feedback}}_{\mathrm{CO2}} + N = \lambda_{\mathrm{Climate+Carbon}} \Delta T + N. \tag{6}$$

To progress, we now wish to evaluate the carbon feedback $\lambda_{\mathrm{Carbon}}$ in terms of changes in ocean and terrestrial carbon inventories.

3. Extracting the Feedback Component to CO_2 Change

A small carbon emission into a preindustrial state, δI_{em} in PgC, is distributed between the atmospheric, ocean, and terrestrial carbon reservoirs (Figure 1a),

$$\delta I_{\mathrm{em}} = \delta I_{\mathrm{atmos}} + \delta I_{\mathrm{ocean}} + \delta I_{\mathrm{ter}} = M \delta \mathrm{CO_2} + V \delta C_{\mathrm{DIC}} + \delta I_{\mathrm{ter}}, \tag{7}$$

where $\delta I_{\mathrm{atmos}} = M\delta\mathrm{CO_2}$ is the change in atmospheric CO_2 inventory since the preindustrial, with M the molar volume of the atmosphere and CO_2 the atmospheric CO_2 mixing ratio; $\delta I_{\mathrm{ocean}} = V\delta C_{\mathrm{DIC}}$ is the change in ocean dissolved inorganic carbon (DIC) inventory, with V the ocean volume and C_{DIC} the mean ocean concentration of DIC; δI_{ter} is the change in terrestrial (soil + vegetation) carbon inventory; and the symbol δ is used to indicate a small infinitesimal change since the preindustrial.

Radiative forcing is related to the log change in atmospheric CO_2, $R_{CO2} = a\Delta \ln CO_2$ (Myhre et al., 2013), so our goal is to find an expression for the change in log CO_2 due to some initial carbon emission, δI_{em}, and subsequent responses to forcing and feedbacks within the atmosphere-ocean-terrestrial carbon system (7). The ocean inventory of carbon involves the DIC concentration C_{DIC}, which may be expressed as a sum of process-driven components (Goodwin et al., 2008; Ito & Follows, 2005; Williams & Follows, 2011) involving the DIC concentration at chemical saturation with atmospheric CO_2, C_{sat}; the disequilibrium concentration at subduction, C_{dis}; and the DIC contribution from regenerated biological material, C_{bio} ($C_{DIC} = C_{sat} + C_{dis} + C_{bio}$; Appendix A). Applying this ocean partitioning allows the perturbation to the global carbon inventory (7) to be reexpressed as

$$\delta I_{em} = \left(I_{atmos} + \frac{VC_{sat}}{B}\right)\delta \ln CO_2 + V\left(\delta C_{dis} + \delta C_{bio} + \frac{\partial C_{sat}}{\partial A_{pre}}\delta A_{pre} + \frac{\partial C_{sat}}{\partial T_{oc}}\delta T_{oc}\right) + \delta I_{ter}, \tag{8}$$

where A_{pre} is the global mean ocean preformed titration alkalinity; T_{oc} is the global mean ocean temperature; $B = \partial \ln CO_2/\partial \ln C_{sat}$ is the Revelle buffer factor of seawater; and $I_{atmos}+(VC_{sat}/B) = I_B$ is the buffered carbon inventory of the air-sea system (Goodwin et al., 2007, 2008, 2015).

Rearranging (8) for $\delta \ln CO_2$, and integrating for large changes using a constant buffered carbon inventory approximation (Goodwin et al., 2007, 2008, 2009, 2011, 2015: Appendix), decomposes ΔR_{CO2} into the initial response to forcing from anthropogenic carbon emissions in the absence of feedbacks, $\Delta R_{CO2}^{forcing}$, plus components from terrestrial and ocean carbon cycle feedbacks, $\Delta R_{CO2}^{feedback} = \Delta R_{terrestrial}^{feedback} + \Delta R_{ocean}^{feedback}$ (Figures 1a and 1b), such that

$$\Delta R_{CO2} = \Delta R_{CO2}^{forcing} + \Delta R_{CO2}^{feedback} = \Delta R_{CO2}^{forcing} + \Delta R_{terrestrial}^{feedback} + \Delta R_{ocean}^{feedback}, \tag{9}$$

where $\Delta R_{CO2}^{forcing}$ is related to terms involving the carbon emission ΔI_{em} and the change in ocean disequilibrium carbon ΔC_{dis} from (8); $\Delta R_{terrestrial}^{feedback}$ is related to the feedback from the change in the terrestrial carbon inventory, ΔI_{ter}; and $\Delta R_{ocean}^{feedback}$ is related to the feedback from the changes in the ocean carbon inventory involving the saturated and regenerated carbon pools (8) from ΔC_{bio}, ΔA_{pre}, and ΔT_{oc} (Appendix A).

4. Evaluating Carbon Feedback From Observational Constraints and Numerical Simulations

4.1. Terrestrial Carbon Feedback

The change in the radiative forcing, $\Delta R_{terrestrial}^{feedback}$ in (9), is related to the change in the cumulative terrestrial carbon inventory relative to the preindustrial, ΔI_{ter} in PgC (Figures 1a and 1b; Goodwin et al., 2007: 2008, 2009, 2011, 2015; Appendix A), which is given by

$$\Delta R_{terrestrial}^{feedback} = -\left(\frac{a}{I_B}\right)\Delta I_{ter}. \tag{10}$$

The terrestrial carbon feedback λ_{Carbon} is diagnosed from reconstructions of the change in the terrestrial carbon inventory and surface temperature record by substituting (10) into (5),

$$\lambda_{Carbon} = -\frac{\Delta R_{terrestrial}^{feedback}}{\Delta T} = -\left(\frac{a}{I_B}\right)\frac{\Delta I_{ter}}{\Delta T}. \tag{11}$$

This new relation (11) is now used to quantify terrestrial carbon feedback from observational reconstructions and Earth system model simulations. λ_{Carbon} is estimated using the following parameters: the radiative forcing coefficient from CO_2, $a = 5.35 \pm 0.27$ W/m^2 (Myhre et al., 2013); the buffered carbon inventory, $I_B = 3451 \pm 96$ PgC (Williams et al., 2017); the global-mean surface temperature change ΔT from the Goddard Institute for Space Studies (GISS) Surface Temperature Analysis (GISTEMP) temperature record (Hansen et al., 2010), including an 11-year average smoothing (Figure 2a, black dotted and full lines); and change in the terrestrial carbon inventory ΔI_{ter} from the Global Carbon Budget (le Quéré et al., 2018; Figure 2b, black). Uncertainties in the terrestrial carbon budget are taken from the additional data for the 16

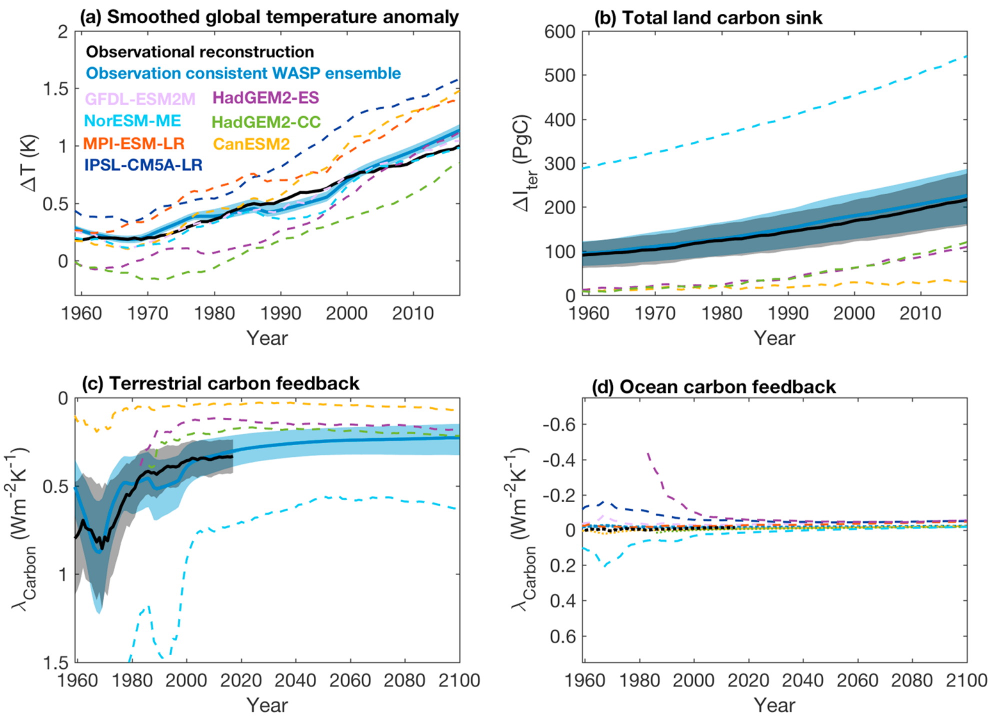

Figure 2. Temperature anomaly, carbon sink, and carbon feedback from observational reconstructions (black: shading is $\pm 1\sigma$ range where shown), observation-constrained WASP simulations (blue: line showing median and shading 66% range), and output from seven CMIP5 Earth system models. (a) Eleven-year running mean surface temperature anomaly relative to pre-1900 average. Observational reconstructions from GISTEMP. (b) Cumulative terrestrial carbon sink. Observational reconstructions from the GCB with additional output from 16 DGVMs to calculate uncertainty. (c) Terrestrial carbon feedback, λ_{Carbon} (equation (11)). Observational reconstructions from GISTEMP and GCB from 1959 to 2017, and simulations using RCP4.5 scenario to project to year 2100. (d) Ocean carbon feedback, λ_{Carbon}, from the CO_2 solubility effect only (dotted lines) and from both ocean biological drawdown and CO_2 solubility effects (dashed lines). Observational reconstructions (black dotted line) derived from Cheng et al. (2017) ocean heat uptake combined with GISTEMP. WASWarming Acidification and Sea level Projector; CMIP5 = Coupled Model Intercomparison Project Phase 5; GISTEMGoddard Institute for Space Studies (GISS) Surface Temperature Analysis; GCB = Global Carbon Budget; DGVMs = dynamic global vegetation models; RCP4.5 = Representative Concentration Pathway 4.5.

individual dynamic global vegetation models (DGVMs) in the Global Carbon Budget (le Quéré et al., 2018; supporting information; Acknowledgments).

These historical reconstructions for the terrestrial carbon inventory and surface temperature reveal an observation-constrained estimate of the terrestrial carbon feedback parameter, $\lambda_{\text{Carbon}} = 0.33 \pm 0.09$ W·m^{-2}·K^{-1} for the present day (Figure 2c, black line and shading), which represents a negative feedback that reduces global warming through terrestrial carbon uptake. The strength of this negative feedback reached a peak magnitude of $\lambda_{\text{Carbon}} = 0.86 \pm 0.34$ W·m^{-2}·K^{-1} in the late 1960s but then has decreased in time as the rate of increase in surface warming since the early 1970s (Figure 2a, black) (Hansen et al., 2010) has not matched the rate of increase in the cumulative terrestrial carbon sink (Figure 2b, black; le Quéré et al., 2018).

The terrestrial carbon feedback is now evaluated from four Coupled Model Intercomparison Project Phase 5 (CMIP5) Earth system models (CanESM2, HadGEM2-ES, HadGEM2-CC, and NorESM-ME), chosen as these have a reliable net export production (nep) variable allowing calculation of ΔI_{ter} in (11). From the simulated ΔI_{ter} and 11-year average ΔT (Figures 2a and 2b), and estimates of a and I_B for each model (Williams et al., 2017), λ_{Carbon} is evaluated from years 1959 to 2100 for the Representative Concentration Pathway 4.5 (RCP4.5) scenario (Figure 2c; Meinshausen et al., 2011). These four CMIP5 Earth system models have a smaller present-day terrestrial carbon feedback parameter ranging from 0.02 to 0.65 W·m^{-2}·K^{-1}, broader than the 1σ range from observational reconstructions (Figure 2c, compare dashed lines to black line and shading). These differences between the Earth system models and the observational estimate arise from their discrepancy between the modeled and observational reconstructions of surface warming and terrestrial carbon uptake (Figures 2a and 2b). The future simulated λ_{Carbon} remains stable under the RCP4.5 scenario, remaining close to the present-day values to year 2100 (Figure 2c).

Additional projections of carbon feedback are made using a very large ensemble of observation-constrained simulations from the Warming Acidification and Sea level Projector (WASP; Goodwin, 2016), for the RCP4.5 scenario (Figure 2, blue line and shading). We adopt the WASP model configuration of Goodwin (2018), with climate feedback including components from different processes operating on different response time scales (Figure 1). An ensemble is generated of many thousands of observation-consistent simulations using the Monte Carlo plus history matching (Williamson et al., 2015) methodology of Goodwin et al. (2018). First, the initial ensemble of 10 million Monte Carlo simulations is generated as in Goodwin (2018), with varied model input parameters, and we integrate each simulation from years 1765 to 2017 with historical forcing. Next the observation-consistency test of Goodwin (2018; see Table 2 therein) is applied with an updated terrestrial carbon range (supporting information Table S1) based on the 16 observation-consistent DGVMs of the Global Carbon Budget 2018 (le Quéré et al., 2018). Only 6,273 simulations pass the observation-consistency test, and a further 3 simulations are rejected as nonphysical since $\lambda_{Climate}$ becomes negative on long time scales.

The remaining ensemble of 6,270 WASP simulations are then consistent with historic observations of surface warming (Figure 2a, compare blue to black), terrestrial carbon uptake (Figure 2b, compare blue to black), and ocean heat content changes (supporting information Table S1; Goodwin, 2018). Due to the observation-simulation agreement in ΔT and ΔI_{ter}, the final WASP ensemble is also in good agreement with the observational reconstructions of terrestrial λ_{Carbon} using (11) from years 1959 to 2017 (Figure 2c, compare blue to black). Under the RCP4.5 scenario, the observation-constrained WASP ensemble shows a similar future behavior as in the response of the CMIP5 models (Figure 2c, compare blue solid line and shading to dashed lines), with λ_{Carbon} displaying only a small change in magnitude from the present day to year 2100.

4.2. Ocean Carbon Feedback

In a similar manner to how the terrestrial carbon feedback is defined relative to ΔI_{ter} (11), the ocean carbon feedback is defined in relation to changes in the ocean DIC from regenerated carbon, ΔC_{bio}, and changes in the ocean saturated carbon inventory from preformed alkalinity ΔA_{pre} and ocean temperature ΔT_{oc} (equations 8 and A8), via

$$\lambda_{Carbon} = -\frac{\Delta R_{ocean}^{feedback}}{\Delta T} = -\left(\frac{a}{I_B}\right)\frac{\Delta C_{bio} + \left(\partial C_{sat}/\partial A_{pre}\right)\Delta A_{pre} + \left(\partial C_{sat}/\partial T_{oc}\right)\Delta T_{oc}}{\Delta T}. \tag{12}$$

This ocean feedback term represents how changes in ocean temperature and ocean biological cycling of carbon and alkalinity from an initial carbon perturbation then feed back to alter the radiative forcing from atmospheric CO_2. Based on Earth system models (evaluating ΔC_{bio}, ΔA_{pre}, and ΔT_{oc}), observational reconstructions for ocean heat uptake (Cheng et al., 2017), and the WASP ensemble (both evaluating ΔT_{oc} only), the ocean carbon feedback is diagnosed as being much smaller than the terrestrial carbon feedback in the present day, ranging from −0.015 to 0.06 $W\cdot m^{-2}\cdot K^{-1}$ (Figures 2c and 2d), and remains small for the 21st century. The magnitude of the ocean carbon feedback might though increase beyond year 2100 due to continued climate-driven changes in ocean temperature, ΔT_{oc}, and ocean biological carbon drawdown, ΔC_{bio}.

Our estimate of ocean carbon feedback (Figure 2d) is much smaller than that implied by Gregory et al. (2009) because the previous approach (Friedlingstein et al., 2006) considers the transient disequilibrium of ocean DIC, C_{dis} (eq. 8), to be part of the ocean carbon feedback, while our method considers C_{dis} as part of the transient ocean response. An idealized feedback grows in magnitude over time, from zero the instant a forcing is applied to some final equilibrium value on long timescales. We do not consider C_{dis} part of the ocean carbon feedback because the time evolution of C_{dis} is the opposite sense: Ocean CO_2 disequilibrium is large the instant CO_2 is emitted into the atmosphere and then decays to zero over long time scales due to ocean carbon uptake (supporting information Figure S1).

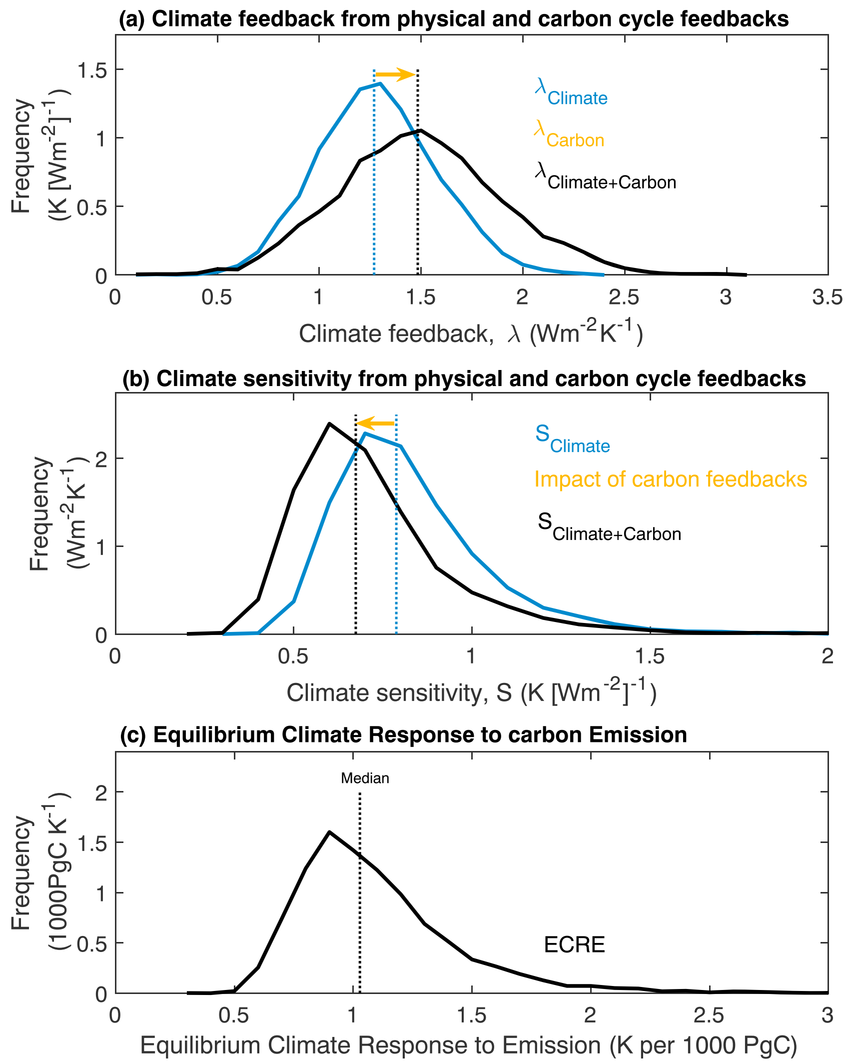

Figure 3. Observational constraints on climate feedback and climate sensitivity from both physical and carbon cycle feedbacks. (a) Climate feedback frequency distributions (solid lines) and median value (dotted lines) for $\lambda_{\mathrm{Climate}}$ (blue) and $\lambda_{\mathrm{Climate+Carbon}} = \lambda_{\mathrm{Climate}} + \lambda_{\mathrm{Carbon}}$ (black). Orange arrow shows the contribution of carbon feedback, $\lambda_{\mathrm{Carbon}}$, to the median values. (b) Climate sensitivity frequency distributions for S_{Climate} (blue) and $S_{\mathrm{Climate+Carbon}}$ (black), with the orange arrow showing impact of carbon feedbacks on the median. (c) Equilibrium Climate Response to carbon Emission (ECRE) frequency distribution (black).

5. Estimating the Combined Carbon-Climate Feedback and Sensitivity

We now place observational constraints on the combined climate plus carbon feedback, $\lambda_{\mathrm{Climate+Carbon}}$, and sensitivity, $S_{\mathrm{Climate+Carbon}}$ in K/(W/m^2), by evaluating both $\lambda_{\mathrm{Climate}}$ and $\lambda_{\mathrm{Carbon}}$ for an idealized perturbation experiment in the observation-constrained WASP ensemble. Each of the 6,270 observation-consistent WASP ensemble members (Figure 2, blue line and shading) is reinitialized at a preindustrial spin-up and integrated for 500 years, forced with an idealized scenario consisting of a 1,000 PgC emission over the first 100 years (Figure 1a).

The total radiative forcing $\Delta R'$ is decomposed into the initial emission forcing, $\Delta R^{\mathrm{forcing}}_{\mathrm{CO2}}$; non-$CO_2$ feedback, $\Delta R^{\mathrm{feedback}}_{\mathrm{non-CO2}}$; and CO_2 feedback, $\Delta R^{\mathrm{feedback}}_{\mathrm{CO2}}$, terms (Figure 1b) using equations (1)–(6). From this decomposition, $\lambda_{\mathrm{Climate}}$ and $\lambda_{\mathrm{Carbon}}$ (Figures 1c ans 1d) are evaluated over multiple response time scales in the observation-consistent ensemble, where the $\lambda_{\mathrm{Climate}}$ results are comparable to the similarly constrained ensemble in Goodwin (2018; see Figure 2 therein). Here $\lambda_{\mathrm{Carbon}}$ in WASP includes both the larger terrestrial and smaller ocean temperature-CO_2 solubility effects (Figure 1d), but WASP does not simulate changes in C_{bio}, which remain small in Earth system models (Figure 2d). For illustration purposes, $\lambda_{Climate}$ and λ_{Carbon} contributions from individual processes are shown by integrating the WASP ensemble with combinations of feedback processes switched off (Figures 1c and 1d, dashed lines are ensemble median values).

Estimates of the carbon and climate feedback parameters, λ_{Carbon} and $\lambda_{Climate}$, applicable on century time scales, are made from the observation-consistent ensemble distributions at the end of the 1,000-PgC emission simulations (Figure 1). The 500-year carbon feedback after a 1,000-PgC emission has a median (and 95% range) of λ_{Carbon} = 0.21 (−0.02 to 0.5) $W{\cdot}m^{-2}{\cdot}K^{-1}$ (Figure 1c), while the physical climate feedback after a 1,000-PgC emission is $\lambda_{Climate}$ = 1.27 (0.73 to 1.88) $W{\cdot}m^{-2}{\cdot}K^{-1}$ (Figures 1b and 3a, blue).

The impact of carbon feedbacks is therefore to increase the overall carbon plus climate feedback above $\lambda_{Climate}$, with an observation-constrained distribution of $\lambda_{Climate+Carbon} = \lambda_{Carbon}+\lambda_{Climate}$ = 1.48 (0.76 to 2.32) $W{\cdot}m^{-2}{\cdot}K^{-1}$ (Figure 3a). Consequently, the climate sensitivity, $S = 1/\lambda$, from non-CO_2 feedbacks alone, $S_{Climate}$ = 0.79 (0.53 to 1.37) $K/(W/m^2)$, is reduced to $S_{Climate+Carbon}$ = 0.67 (0.43 to 1.32) $K/(W/m^2)$, when encapsulating both non-CO_2 and CO_2 feedbacks acting together (Figure 3b). This estimate of $S_{Climate+Carbon}$ (Figure 3b, black) represents the total sensitivity of the climate system to perturbation by carbon emission over century time scales, including both physical climate and carbon-cycle feedbacks.

6. Conclusions

A new method is presented to constrain the carbon feedback parameter, finding for the present-day terrestrial carbon system $\lambda_{Carbon} = 0.33 \pm 0.09$ $W{\cdot}m^{-2}{\cdot}K^{-1}$ (Figure 2c) based on observational reconstructions of carbon uptake and warming (Hansen et al., 2010; le Quéré et al., 2018) and λ_{Carbon} = 0.02 to 0.65 $W{\cdot}m^{-2}{\cdot}K^{-1}$ in four CMIP5 models. This compares to a previous method implying terrestrial carbon feedback of $\lambda_{Carbon} = 0.7 \pm 0.5$ $W{\cdot}m^{-2}{\cdot}K^{-1}$, based on analysis of the earlier Coupled Climate-Carbon Cycle Model Intercomparison Project (C4MIP) climate model ensemble (Arneth et al., 2010; Friedlingstein et al., 2006; Gregory et al., 2009) and comprising a linearization of separate CO_2-carbon (1.1 ± 0.5 $W{\cdot}m^{-2}{\cdot}K^{-1}$) and climate-carbon (−0.4 ± 0.2 $W{\cdot}m^{-2}{\cdot}K^{-1}$) components. The linearization assumed by the previous method introduces errors (Arora et al., 2013; Schwinger et al., 2014), and this means the method cannot be applied to observational reconstructions. To avoid making the linearization assumption, and so be applicable to observational reconstructions, our method assumes a constant buffered carbon inventory (Appendix A), a good approximation for carbon perturbations up to ~5,000 PgC or for atmospheric CO_2 reaching ~1,100 ppm (Goodwin et al., 2007, 2008, 2009).

The Equilibrium Climate Response to Emission (ECRE), in K/1,000 PgC, expresses the warming per unit carbon emitted once ocean heat uptake approaches zero over centennial to multicentennial time scales, ECRE = $\Delta T/\Delta I_{em}$ (Frölicher & Paynter, 2015). This atmosphere-ocean equilibrium is approached over many centuries, but not necessarily reached due to the effect of other longer time scale carbon and climate feedbacks, such as from ice sheet-albedo feedbacks (Rohling et al., 2018) and multimillennial $CaCO_3$ sediment and weathering responses (Archer, 2005). In the absence of carbon feedbacks, Williams et al. (2012) related the ECRE to climate feedback, $\lambda_{Climate}$, via ECRE = $a/(\lambda_{Climate} I_B)$. Here we extend the relationship to include the effects of both climate and carbon feedbacks, ECRE = $a/(\lambda_{Climate+Carbon} I_B)$, applicable after ocean CO_2 invasion and heat uptake but prior to significant $CaCO_3$ sediment and weathering responses (Archer, 2005; Goodwin et al., 2007, 2008, 2015). Our historically constrained feedback estimates (Figures 3a and 3b) imply ECRE =1.0 (0.6 to 2.0) K/1,000 PgC emitted (Figure 3c), with the upper half of our range (from 1 to 2 K/1,000 PgC) consistent with a CMIP5-based estimate (Frölicher & Paynter, 2015). Carbon and climate feedbacks not constrained historically (e.g., MacDougall & Knutti, 2016; Pugh et al., 2018; Rohling et al., 2018; Zickfeld et al., 2013) may alter future $\lambda_{Climate+Carbon}$ and so alter ECRE. We anticipate this relationship, ECRE = $a/(\lambda_{Climate+Carbon} I_B)$, will be useful in elucidating how different carbon and climate feedbacks contribute to the multicentury warming response to carbon emission.

Appendix A: Connecting Radiative Feedbacks to Changes in Carbon Inventories

Our aim is to separate the total CO_2 radiative forcing into a sum of linearly separable terms representing different processes and feedbacks. We start by considering how carbon emissions perturb carbon storage across the atmosphere-ocean-terrestrial system. We now write identities for the changes in atmospheric and ocean carbon inventories containing terms with $\delta\ln CO_2$. Using the identity for small perturbations in x, $\delta x = x\delta\ln x$, we write an identity for a small perturbation in atmospheric CO_2 inventory, δI_{atmos}, in terms of a small perturbation to the logarithm of atmospheric CO_2, $\delta\ln CO_2$,

$$\delta I_{\mathrm{atmos}} = I_{\mathrm{atmos}}\delta\ln\mathrm{CO_2}, \tag{A1}$$

where I_{atmos} is the initial atmospheric CO_2 inventory at the unperturbed preindustrial state.

The change in ocean DIC is considered, via a process-driven viewpoint (Goodwin et al., 2008; Ito & Follows, 2005; Williams & Follows, 2011), in terms of the sum of components from the change in chemically saturated DIC arising from changes in atmospheric CO_2 and seawater properties, δC_{sat}; the change in chemical disequilibrium of ocean DIC relative to atmospheric CO_2, δC_{dis}; and the combined change in ocean DIC from regenerated soft tissue and $CaCO_3$ drawdown, δC_{bio}:

$$\delta C_{\mathrm{DIC}} = \delta C_{\mathrm{sat}} + \delta C_{\mathrm{dis}} + \delta C_{\mathrm{bio}}. \tag{A2}$$

Due to the carbonate chemistry system, the perturbation to C_{sat} is a function of the change to the logarithm of atmospheric CO_2, $\delta\ln CO_2$; the change in mean ocean preformed titration alkalinity, δA_{pre}; the change in mean seawater temperature, δT_{oc}; and the change in mean seawater salinity, δS: $\delta C_{sat} = \delta C_{sat}(\delta\ln CO_2, \delta A_{pre}, \delta T_{oc}, \delta S)$. This small perturbation to C_{sat} is now expanded after Goodwin and Lenton (2009) into components from $\delta\ln CO_2$, δA_{pre}, δT_{oc}, and δS:

$$\delta C_{\mathrm{dis}} = \frac{\partial C_{\mathrm{sat}}}{\partial\ln\mathrm{CO_2}}\delta\ln\mathrm{CO_2} + \frac{\partial C_{\mathrm{sat}}}{\partial A_{\mathrm{pre}}}\delta A_{\mathrm{pre}} + \frac{\partial C_{\mathrm{sat}}}{\partial T_{\mathrm{oc}}}\delta T_{\mathrm{oc}} + \frac{\partial C_{\mathrm{sat}}}{\partial S}\delta S, \tag{A3}$$

where the salinity term, $(\partial C_{sat}/\partial S)\delta S$, is small and henceforth will be omitted.

Again, using the identity for small perturbations in a variable x, $\delta x = x\delta\ln x$, but applying to C_{sat}, the term for the sensitivity of C_{sat} to $\ln CO_2$ in (A3) becomes

$$\frac{\partial C_{\mathrm{sat}}}{\partial\ln\mathrm{CO_2}}\delta\ln\mathrm{CO_2} = C_{\mathrm{sat}}\frac{\partial\ln C_{\mathrm{sat}}}{\partial\ln\mathrm{CO_2}}\delta\ln\mathrm{CO_2} = \frac{C_{\mathrm{sat}}}{B}\delta\ln\mathrm{CO_2}, \tag{A4}$$

where $B = (\partial\ln CO_2/\partial\ln C_{sat})$ is the Revelle buffer factor expressing how fractional chemical in atmospheric CO_2 is much larger than fractional changes in DIC with B, the order 10 for the present ocean (e.g., Williams & Follows, 2011). Substituting (A4) into (A3), and noting that $I_{ocean} = VC_{DIC}$, produces an identity for δI_{ocean} containing a term in $\delta\ln CO_2$:

$$\delta I_{\mathrm{ocean}} = \frac{I^{\mathrm{sat}}_{\mathrm{ocean}}}{B}\delta\ln\mathrm{CO_2} + V\left(\delta C_{\mathrm{dis}} + \delta C_{\mathrm{bio}} + \frac{\partial C_{\mathrm{sat}}}{\partial A_{\mathrm{pre}}}\delta A_{\mathrm{pre}} + \frac{\partial C_{\mathrm{sat}}}{\partial T_{\mathrm{oc}}}\delta T_{\mathrm{oc}}\right), \tag{A5}$$

where $I^{sat}_{ocean} = VC_{sat}$ is the ocean inventory of saturated DIC at current atmospheric CO_2. Substituting δI_{ocean} (A5) and δI_{atmos} (A1) into (7), and rearranging to solve for the log change in atmospheric CO_2 mixing ratio to small perturbations to I_{em}, I_{ter}, C_{dis}, C_{bio}, A_{pre}, and T_{oc}, reveals

$$\left(I_{\mathrm{atmos}} + \frac{I^{\mathrm{sat}}_{\mathrm{ocean}}}{B}\right)\delta\ln\mathrm{CO_2} = \delta I_{\mathrm{em}} - \delta I_{\mathrm{ter}} - V\left(\delta C_{\mathrm{dis}} + \delta C_{\mathrm{bio}} + \frac{\partial C_{\mathrm{sat}}}{\partial A_{\mathrm{pre}}}\delta A_{\mathrm{pre}} + \frac{\partial C_{\mathrm{sat}}}{\partial T_{\mathrm{oc}}}\delta T_{\mathrm{oc}}\right) \tag{A6}$$

The issue now is that this identity for $\delta\ln CO_2$ (A7) applies only to small infinitesimal perturbations, and we wish to solve for the change in log CO_2 for large finite perturbations. The next step is therefore to integrate (A6) over large finite perturbations in I_{em}, I_{ter}, C_{dis}, C_{bio}, A_{pre}, and T_{oc}.

To integrate (A6), we note that the left-hand side contains the buffered carbon inventory, I_B (Goodwin et al., 2007, 2008), defined as the atmospheric carbon inventory added to the ocean saturated-DIC inventory divided by the Revelle buffer factor, $I_B = I_{\text{atmos}} + \left(I^{\text{sat}}_{\text{ocean}}/B\right)$. I_B represents the total buffered CO_2 and DIC in the atmosphere-ocean system that is available for redistribution between the CO_2 and carbonate ion pools (Goodwin et al., 2009), given that the majority of ocean DIC is in the form of bicarbonate ions. At the preindustrial state, $I_B = 3{,}451 \pm 96$ PgC in the CMIP5 models analyzed by Williams et al. (2017).

Using this constant buffered carbon inventory approach (supporting information), we integrate (A6) to find the change in atmospheric CO_2 for large finite perturbations to total carbon emitted, ΔI_{em}; the change in terrestrial carbon storage, ΔI_{ter}; and the large changes in mean ocean values of ΔC_{dis}, ΔC_{bio}, ΔA_{pre}, and ΔT_{oc}, so that

$$I_B \Delta \ln CO_2 = \Delta I_{\text{em}} - \Delta I_{\text{ter}} - V\left(\Delta C_{\text{dis}} + \Delta C_{\text{bio}} + \frac{\partial C_{\text{sat}}}{\partial A_{\text{pre}}}\Delta A_{\text{pre}} + \frac{\partial C_{\text{sat}}}{\partial T_{\text{oc}}}\Delta T_{\text{oc}}\right). \quad \text{(A7)}$$

Multiplying (A7) by the CO_2-radiative forcing coefficient, a, produces an expression for the radiative forcing from CO_2 in (9),

$$\Delta R_{CO2} = \Delta R^{\text{forcing}}_{CO2} + \Delta R^{\text{feedback}}_{\text{terrestrial}} + \Delta R^{\text{feedback}}_{\text{ocean}},$$

as a sum of separable terms representing different processes, each linked to a different change in a carbon inventory. The CO_2 radiative forcing,

$$\Delta R^{\text{forcing}}_{CO2} = (a/I_B)(\Delta I_{\text{em}} - V\Delta C_{\text{dis}}), \quad \text{(A8a)}$$

represents the direct effect of the emitted carbon partitioned between the atmosphere and ocean, including both chemical equilibrium (ΔI_{em}) and the transient chemical disequilibrium between the atmosphere and ocean (ΔC_{dis}) of the carbon emitted, but without subsequent carbon feedbacks. The radiative forcing from the carbon feedbacks for the terrestrial,

$$\Delta R^{\text{feedback}}_{\text{terrestrial}} = -(a/I_B)\Delta I_{\text{ter}}, \quad \text{(A8b)}$$

depends on the change in terrestrial carbon storage since the preindustrial, and that for the ocean,

$$\Delta R^{\text{feedback}}_{\text{ocean}} = -(a/I_B)V\left(\Delta C_{\text{bio}} + \left[\partial C_{\text{sat}}/\partial A_{\text{pre}}\right]\Delta A_{\text{pre}} + \left[\partial C_{\text{sat}}/\partial T_{\text{oc}}\right]\Delta T_{\text{oc}}\right), \quad \text{(A8c)}$$

depends on the changes to the ocean biological drawdown of soft tissue and $CaCO_3$, including the titration alkalinity effects, and on the changes in the seawater temperature since the preindustrial, altering the solubility of CO_2 in seawater.

Acknowledgments
We acknowledge global surface temperature anomaly data from GISTEMP Team, 2018: GISS Surface Temperature Analysis (GISTEMP), NASA Goddard Institute for Space Studies. Data set was accessed 16 January 2018 at https://data.giss.nasa.gov/gistemp/. We acknowledge the Global Carbon Project's Global Carbon Budget 2018 for the land carbon sink data, including the multimodel mean from 16 DGVMs from years 1750 to 1959 and the model breakdowns from these models from years 1959 to 2017. We thank Stephen Sitch for providing additional data from these 16 Global Carbon Project DGVMs prior to 1959, allowing the intermodel standard deviation in the intermodel cumulative land carbon sink, ΔI_{ter}, to be calculated. The authors acknowledge the World Climate Research Programmes Working Group on Coupled Modelling responsible for CMIP5. This work was funded by UK NERC Grant NE/N009789/1 and combined UK NERC/UK Government Department of BEIS Grant NE/P01495X/1.

References

Andrews, T., Gregory, J. M., & Webb, M. J. (2015). The dependence of radiative forcing and feedback on evolving patterns of surface temperature change in climate models. *Journal of Climate*, *28*(4), 1630–1648. https://doi.org/10.1175/JCLI-D-14-00545.1

Andrews, T., Gregory, J. M., Webb, M. J., & Taylor, K. E. (2012). Forcing, feedbacks and climate sensitivity in CMIP5 coupled atmosphere-ocean climate models. *Geophysical Research Letters*, *39*, L09712. https://doi.org/10.1029/2012GL051607

Archer, D. (2005). Fate of fossil fuel CO_2 in geologic time. *Journal of Geophysical Research*, *110*, C09S05. https://doi.org/10.1029/2004JC002625

Armour, K. C., Bitz, C. M., & Roe, G. H. (2013). Time-varying climate sensitivity from regional feedbacks. *Journal of Climate*, *26*(13), 4518–4534. https://doi.org/10.1175/JCLI-D-12-00544.1

Arneth, A., Harrison, S. P., Zaehle, S., Tsigaridis, K., Menon, S., Bartlein, P. J., et al. (2010). Terrestrial biogeochemical feedbacks in the climate system. *Nature Geoscience*, *3*(8), 525–532. https://doi.org/10.1038/ngeo905

Arora, V. K., Boer, G. J., Friedlingstein, P., Eby, M., Jones, C. D., Christian, J. R., et al. (2013). Carbon–concentration and carbon–climate feedbacks in CMIP5 Earth system models. *Journal of Climate*, *26*(15), 5289–5314. https://doi.org/10.1175/JCLI-D-12-00494.1

Ceppi, P., & Gregory, J. M. (2017). Relationship of tropospheric stability to climate sensitivity and Earth's observed radiation budget. *Proceedings of the National Academy of Sciences*, *114*(50), 13,126–13,131. https://doi.org/10.1073/pnas.1714308114

Cheng, L., Trenberth, K. E., Fasullo, J., Boyer, T., Abraham, J., & Zhu, J. (2017). Improved estimates of ocean heat content from 1960 to 2015. *Science Advances*, *3*(3), e1601545. https://doi.org/10.1126/sciadv.1601545

Friedlingstein, P., Cox, P., Betts, R., Bopp, L., von Bloh, W., Brovkin, V., et al. (2006). Climate–carbon cycle feedback analysis: Results from the C4MIP model intercomparison. *Journal of Climate*, *19*(14), 3337–3353. https://doi.org/10.1175/JCLI3800.1

Friedlingstein, P., Dufresne, J. L., Cox, P. M., & Rayner, P. (2003). How positive is the feedback between climate change and the carbon cycle? *Tellus B*, *55*(2), 692–700. https://doi.org/10.1034/j.1600-0889.2003.01461.x

Frölicher, T. L., & Paynter, D. J. (2015). Extending the relationship between global warming and cumulative carbon emissions to multi-millennial timescales. *Environmental Research Letters*, *10*(7), 075002.

Goodwin, P. (2016). How historic simulation-observation discrepancy affects future warming projections in a very large model ensemble. *Climate Dynamics*, CLDY-D-15-00368R2. https://doi.org/10.1007/s00382-015-2960-z

Goodwin, P. (2018). On the time evolution of climate sensitivity and future warming. *Earth's Future*, *6*, 1336–1348. https://doi.org/10.1029/2018EF000889

Goodwin, P., Follows, M. J., & Williams, R. G. (2008). Analytical relationships between atmospheric carbon dioxide, carbon emissions, and ocean processes. *Global Biogeochemical Cycles*, *22*, GB3030. https://doi.org/10.1029/2008GB003184

Goodwin, P., Katavouta, A., Roussenov, V. M., Foster, G. L., Rohling, E. J., & Williams, R. G. (2018). Pathways to 1.5 and 2 °C warming based on observational and geological constraints. *Nature Geoscience*, *11*(2), 102–107. https://doi.org/10.1038/s41561-017-0054-8

Goodwin, P., & Lenton, T. (2009). Quantifying the feedback between ocean heating and CO_2 solubility as an equivalent carbon emission. *Geophysical Research Letters*, *36*, L15609. https://doi.org/10.1029/2009GL039247

Goodwin, P., Oliver, K. I. C., & Lenton, T. M. (2011). Observational constraints on the causes of Holocene CO_2 change. *Global Biogeochemical Cycles*, *25*, GB3011. https://doi.org/10.1029/2010GB003888

Goodwin, P., Williams, R. G., Follows, M. J., & Dutkiewicz, S. (2007). Ocean-atmosphere partitioning of anthropogenic carbon dioxide on centennial timescales. *Global Biogeochemical Cycles*, *21*, GB1014. https://doi.org/10.1029/2006GB002810

Goodwin, P., Williams, R. G., & Ridgwell, A. (2015). Sensitivity of climate to cumulative carbon emissions due to compensation of ocean heat and carbon uptake. *Nature Geoscience*, *8*(1), 29–34. https://doi.org/10.1038/ngeo2304

Goodwin, P., Williams, R. G., Ridgwell, A., & Follows, M. J. (2009). Climate sensitivity to the carbon cycle modulated by past and future changes in ocean chemistry. *Nature Geoscience*, *2*(2), 145–150. https://doi.org/10.1038/ngeo416

Gregory, J. M., Ingram, W. J., Palmer, M. A., Jones, G. S., Stott, P. A., Thorpe, R. B., et al. (2004). A new method for diagnosing radiative forcing and climate sensitivity. *Geophysical Research Letters*, *31*, L03205. https://doi.org/10.1029/2003GL018747

Gregory, J. M., Jones, C. D., Cadule, P., & Friedlingstein, P. (2009). Quantifying carbon cycle feedbacks. *Journal of Climate*, *22*(19), 5232–5250. https://doi.org/10.1175/2009JCLI2949.1

Hansen, J., Ruedy, R., Sato, M., & Lo, K. (2010). Global surface temperature change. *Reviews of Geophysics*, *48*, RG4004. https://doi.org/10.1029/2010RG000345

Intergovernmental Panel on Climate Change (2013). In T. F. Stocker, et al. (Eds.), *Climate Change 2013: The physical science basis*. Cambridge: Cambridge University Press.

Ito, T., & Follows, M. J. (2005). Preformed phosphate, soft tissue pump and atmospheric CO_2. *Journal of Marine Research*, *63*(4), 813–839. https://doi.org/10.1357/0022240054663231

Knutti, R., Rugenstein, M. A. A., & Hergerl, G. C. (2017). Beyond equilibrium climate sensitivity. *Nature Geoscience*, *10*(10), 727–736. https://doi.org/10.1038/ngeo3017

le Quéré, C., Andrew, R. M., Friedlingstein, P., Sitch, S., Pongratz, J., Manning, A. C., et al. (2018). Global carbon budget 2017. *Earth System Science Data*, *10*(1), 405–448. https://doi.org/10.5194/essd-10-405-2018

MacDougall, A. H., & Knutti, R. (2016). Projecting the release of carbon from permafrost soils using a perturbed physics ensemble modelling approach. *Biogeosciences*, *13*, 2123–2136. https://doi.org/10.5194/bg-13-2123-2016

Meinshausen, M., Smith, S. J., Calvin, K., Daniel, J. S., Kainuma, M. L. T., Lamarque, J. F., et al. (2011). The RCP greenhouse gas concentrations and their extensions from 1765 to 2300. *Climatic Change*, *109*(1-2), 213–241. https://doi.org/10.1007/s10584-011-0156-z

Myhre, G., Shindell, D., Bréon, F.-M., Collins, W., Fuglestvedt, J., Huang, J., et al. (2013). Anthropogenic and natural radiative forcing supplementary material. In T. F. Stocker, D. Qin, G.-K. Plattner, M. Tignor, S. K. Allen, J. Boschung, et al. (Eds.), *Climate Change 2013: The physical science basis. Contribution of Working Group I to the Fifth Assessment Report of the Intergovernmental Panel on Climate Change* (Chap. 8, pp. 659–740). Cambridge: Cambridge University Press.

Pugh, T. A. M., Jones, C. D., Huntingford, C., Burton, C., Arneth, A., Brovkin, V., et al. (2018). A large committed long-term sink of carbon due to vegetation dynamics. *Earth's Future*, *6*, 1413–1432. https://doi.org/10.1029/2018EF000935

Rohling, E. J., Marino, G., Foster, G. L., Goodwin, P. A., von der Heydt, A. S., & Köhler, P. (2018). Comparing climate sensitivity, past and present. *Annual Review of Marine Science*, *10*(1), 261–288. http://www.annualreviews.org/doi/full/10.1146/annurev-marine-121916-063242

Schwinger, J., Tjiputra, J. F., Heinze, C., Bopp, L., Christian, J. R., Gehlen, M., et al. (2014). Nonlinearity of ocean carbon cycle feedbacks in CMIP5 Earth system models. *Journal of Climate*, *27*(11), 3869–3888. https://doi.org/10.1175/JCLI-D-13-00452.1

Williams, R. G., & Follows, M. J. (2011). *Ocean dynamics and the carbon cycle: Principles and mechanisms* (p. 416). Cambridge: Cambridge University Press. https://doi.org/10.1017/CBO9780511977817

Williams, R. G., Goodwin, P., Ridgwell, A., & Woodworth, P. L. (2012). How warming and steric sea level rise relate to cumulative carbon emissions. *Geophysical Research Letters*, *39*, L19715. https://doi.org/10.1029/2012GL052771

Williams, R. G., Roussenov, V., Goodwin, P., Resplandy, L., & Bopp, L. (2017). Sensitivity of global warming to carbon emissions: Effects of heat and carbon uptake in a suite of Earth system models. *Journal of Climate*, *30*(23), 9343–9363. https://doi.org/10.1175/JCLI-D-16-0468.1

Williamson, D., Blaker, A. T., Hampton, C., & Salter, J. (2015). Identifying and removing structural biases in climate models with history matching. *Climate Dynamics*, *45*(5-6), 1299–1324. https://doi.org/10.1007/s00382-014-2378-z

Zickfeld, K., Eby, M., Weaver, A. J., Alexander, K., Crespin, E., Edwards, N. R., et al. (2013). Long-term climate change commitment and reversibility: An EMIC intercomparison. *Journal of Climate*, *26*(16). https://doi.org/10.1175/JCLI-D-12-00584.1